A Global Statistical–Dynamical Tropical Cyclone Wind Radii Forecast Scheme

JOHN A. KNAFF

NOAA/Center for Satellite Application and Research, Fort Collins, Colorado

CHARLES R. SAMPSON

Naval Research Laboratory, Monterey, California

GALINA CHIROKOVA

Cooperative Institute for Research in the Atmosphere, Fort Collins, Colorado

(Manuscript received 15 September 2016, in final form 16 December 2016)

ABSTRACT

Forecasts of tropical cyclone (TC) surface wind structure have recently begun to show some skill, but the number of reliable forecast tools, mostly regional hurricane and select global models, remains limited. To provide additional wind structure guidance, this work presents the development of a statistical–dynamical method to predict tropical cyclone wind structure in terms of wind radii, which are defined as the maximum extent of the 34-, 50-, and 64-kt (1 kt = 0.514 m s^{-1}) winds in geographical quadrants about the center of the storm. The basis for TC size variations is developed from an infrared satellite-based record of TC size, which is homogenously calculated from a global sample. The change in TC size is predicted using a statistical–dynamical approach where predictors are based on environmental diagnostics derived from global model forecasts and observed storm conditions. Once the TC size has been predicted, the forecast intensity and track are used along with a parametric wind model to estimate the resulting wind radii. To provide additional guidance for applications and users that require forecasts of central pressure, a wind–pressure relationship that is a function of TC motion, intensity, wind radii (i.e., size), and latitude is then applied to these forecasts. This forecast method compares well with similar wind structure forecasts made by global forecast and regional hurricane models and when these forecasts are used as a member of a simple consensus; its inclusion improves the forecast performance of the consensus.

1. Introduction

The estimation and forecast of surface winds associated with tropical cyclones (TCs) is important to a variety of stakeholders and applications. Important stakeholders include state and local governments, private industry, and the U.S. military. Key applications include wind-based risks and impacts, and wave and surge forecasting. The National Hurricane Center (NHC), the Central Pacific Hurricane Center (CPHC), and the Joint Typhoon Warning Center (JTWC) provide information about TC risks and make 6-hourly forecasts of TC tracks, intensities, and wind structures for all active TCs. The initial and forecast TC surface wind structures are provided in terms of the maximum radial extent of 34-, 50- and 64-kt (1 kt = 0.514 m s^{-1}), or gale force (R34), damaging (R50) and hurricane (R64) force winds in geographic quadrants surrounding the TC. These are collectively referred to as wind radii. NHC also has been conducting postseason reanalysis or best tracking of their wind radii since 2004. The operational units for intensity are knots and for wind radii they are nautical miles (n mi, 1 n mi = 1.85 km), so these units will be used throughout this paper.

As of 2016, NHC and the JTWC forecast R64 through 36 h, and R50 and R34 wind radii through 72 h, while intensity and track are forecast through 120 h (Knaff and Sampson 2015). Recent work has shown that the current NHC forecasts are skillful to NHC's maximum lead time of 72 h (Knaff and Sampson 2015; Cangialosi and Landsea 2016). However, because best-tracked wind radii have been considered to have large subjectively determined uncertainty (Landsea and Franklin 2013), NHC does not yet routinely verify their wind radii forecasts (Knaff and

Corresponding author e-mail: John Knaff, john.knaff@noaa.gov

DOI: 10.1175/WAF-D-16-0168.1

Harper 2010; Cangialosi and Landsea 2016). Nonetheless, independently Knaff et al. (2016) and Dolling et al. (2016) reached the same conclusion that the best-tracked wind radii are reasonable and useful estimates of the wind structure that are reliable enough for technique development. This approach is also used in this work.

Operational guidance on forecast wind radii comes primarily from numerical weather prediction (NWP) models and purely statistical models, like the wind radii climatology and persistence model (DRCL; Knaff et al. 2007, hereafter K07). NWP comes from a combination of regional hurricane specific models and global models (NHC 2009; CIRA 2016b). Wind radii are estimated by software developed at the Geophysical Research Laboratory that tracks the storm center, intensity, and wind radii in the model output; the process has been described by Marchok (2002) and more recently by Tallapragada et al. (2014). While NWP initially struggled to produce skillful wind radii forecasts (see Knaff et al. 2006), Sampson and Knaff (2015) recently showed that a consensus of NWP 34-kt wind radii forecasts provides skillful (vs DRCL) guidance through 120 h. However, individual NWP models are often biased and still struggle to show skill relative to climatology and persistence when predicting wind radii.

A similar historical analogy exists for tropical cyclone intensity forecasts. Many of the early advances in TC intensity forecast skill were due to a combination of regional NWP (e.g., Bender et al. 2007; Bernardet et al. 2015) and statistical–dynamical approaches (e.g., DeMaria et al. 2005; DeMaria 2009; DeMaria et al. 2007, 2014). The statistical–dynamical approach combines forecast information from a dynamical model within a statistical framework to make, typically more specific or smaller-scale, forecasts. A good example of this approach is the model output statistics that have long provided forecasts for specific locations based on numerical model forecast output (Carter et al. 1989). It has been shown that intensity forecasts made with the statistical–dynamical methods often produced the most skillful (vs climatology and persistence) individual intensity forecasts. However, it was a simple equally weighted consensus approach (Sampson et al. 2008) that ultimately proved most skillful for intensity forecasts (DeMaria et al. 2014).

At this time, there is a notable absence of models that use a statistical–dynamical approach to provide wind radii guidance in research and in operations. With this deficiency in mind, and a desire to have more relatively independent members available for consensus methods, this study will describe a statistical–dynamical approach to making wind radii forecasts in hopes that wind radii forecasts can be further improved by using the combination of NWP and statistical–dynamical approaches.

2. Data and methodology

a. The dependent variable

To build a statistical model designed to predict TC structure changes, some thought was needed concerning the dependent variable $Y = f(x_i)$, where x_i's are the independent variables or predictors. For wind radii the following considerations were important. The variable Y must provide information about the primary vortex size, be available for all intensity ranges, be valid over landmasses, and be consistent in all ocean basins—noting that operational procedures (Knaff et al. 2003; Rappaport et al. 2009) and the quality of the wind radii have been shown to vary over time and by basin (K07). In addition, it also is desirable to estimate a single homogeneously developed Y, rather than build a model for several instances of Y (e.g., one for each radii, each quadrant, MSLP, etc.) or Y's that were estimated in different ways and/or have variable quality. It also quickly becomes rather cumbersome to maintain and occasionally update 3–12 regressions at 20 lead times, as was the case for the McAdie wind radii climatology and persistence model (MRCL) discussed in K07. Our choice of homogeneously calculated Y for this work is the temporal change from the initial time of a normalized infrared (IR) satellite-based TC size estimate R5,[1] developed in Knaff et al. (2014b, hereafter K14). We will refer to this Y, whose development is described next, as ΔF_{R5}.

The first step in creating ΔF_{R5} is to account for the variations of R5 with TC intensity and create the normalized TC size variable F_{R5}. This is done by dividing R5 by an intensity-based climatology $R5_c$ (see Knaff et al. 2014a), where VM is the intensity in knots, as shown in Fig. 1:

$$R5_c = 7.653 + \left(\frac{VM}{11.651}\right) - \left(\frac{VM}{59.067}\right)^2, \qquad (1)$$

where $R5_c$ has units of degrees latitude, increasing from about 9° latitude (999 km) at 20-kt intensities to 13° latitude (1443 km) at 90 kt. At intensities greater than 90 kt, $R5_c$ eventually maximizes at 14° latitude (1554 km),

[1] We define R5 as the radius at which the TC wind field is indistinguishable from the background flow in a climatological environment (K14) and has units of degrees latitude. R5 is calculated from estimates of the tangential wind at 500-km radius (V500) that are based on the principle components of the azimuthally averaged storm-centered IR brightness temperatures and the sine of the absolute value of latitude, which follows similar approaches used by Mueller et al. (2006) and Kossin et al. (2007). Full details can be found in Knaff et al. (2014b).

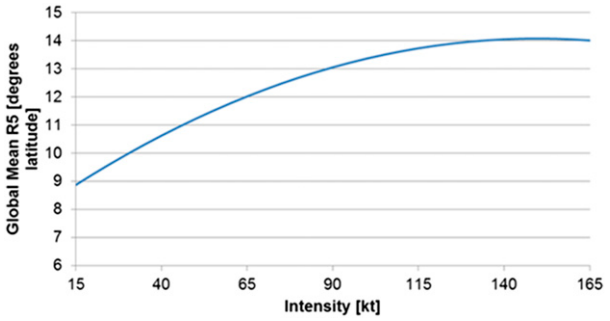

FIG. 1. Graph of the intensity-based climatology of TC size $R5_c$ (° latitude) as a function of TC intensity (kt).

actually decreasing a tiny bit for the most intense storms. A similar pattern of behavior was noted for 34-kt wind radii observed in the western North Pacific (Wu et al. 2015), where the 34-kt wind radii leveled off at approximately 775 km. The normalization procedure is

$$F_{R5} = R5/R5_c. \quad (2)$$

To provide the reader a visual example of what a time series of R5 and F_{R5} would look like for a hurricane, Fig. 2 shows the R5 and F_{R5} time series for east Pacific Hurricane Amanda (2014). Amanda was a relatively short-lived major TC with a life cycle of just 7½ days. During that time, it reached a peak intensity of 135 kt, making it the strongest east Pacific hurricane to occur in the month of May (Stewart 2014). To accompany these time series, IR images of the storm are shown at 24-h intervals starting at 0000 UTC 23 May. These results show the changes in TC structure that accompany the variations of R5 and F_{R5}. Having estimated F_{R5} for all the cases available, the last step is to create our dependent variable, ΔF_{R5}, as a function of forecast lead time.

To form $\Delta F_{R5}(t)$, the initial value of $F_{R5}(t = 0)$ is subtracted from the value of F_{R5} for each 6-hourly lead time from 6 to 120 h. The $\Delta F_{R5}(t)$ values were then created for the following global tropical cyclone basins: the North Atlantic (NATL), the eastern and central North Pacific (EPAC), the western North Pacific and north Indian Ocean (WPAC), and the Southern Hemisphere (SHEM). The north Indian Ocean has too few cases to develop this capability, and we could have combined that basin with the WPAC, but that was not done in this study. The years 1996–2012 were used in the NATL and EPAC and years 2001–12 were used in the WPAC and SHEM. The availability of IR imagery in the WPAC and SHEM limited the starting year. The resulting numbers of cases available for model development are similar for all these basins, as shown in Table 1.

b. *Fitting the statistical–dynamical model*

Statistical–dynamical model development follows past work with intensity forecasting, where the change in intensity from the initial time is used as the dependent variable and independent variables or predictors are

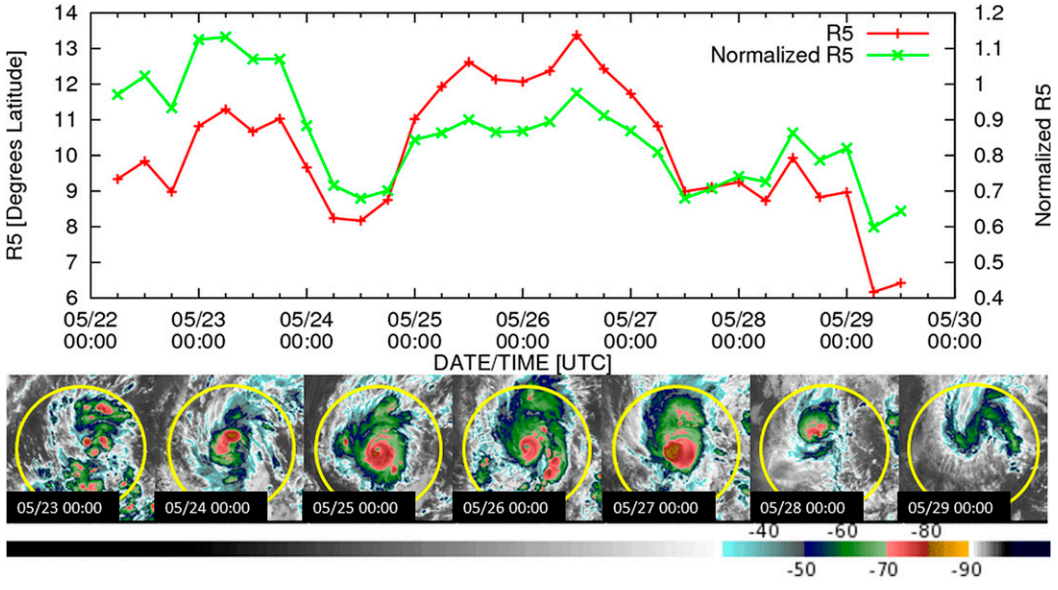

FIG. 2. (top) Example of the 3-hourly time series of TC size, R5, and normalized TC size F_{R5}, for Hurricane Amanda (2014). (bottom) Daily, color enhanced IR images (°C) corresponding to the estimates of R5 beginning at 0000 UTC 23 May. A yellow circle is located at a range of 500 km from the TC center, and the color enhancement is provided below the images.

TABLE 1. Number of cases available for multiple linear regression development in the NATL, EPAC, WPAC, and SHEM basins.

Lead time (h)	NATL	EPAC	WPAC	SHEM
6	5915	4613	5168	4554
12	5724	4453	4986	4390
18	5498	4265	4777	4204
24	5448	4055	4563	4010
30	4993	3824	4347	3815
36	4743	3594	4136	3618
42	4499	3367	3927	3424
48	4262	3145	3723	3237
54	4041	2933	3527	3052
60	3827	2726	3337	2873
66	3621	2524	3151	2699
72	3425	2329	2967	2531
78	3238	2145	2988	2369
84	3058	1972	2610	2217
90	2891	1808	2438	2068
96	2731	1656	2268	1922
102	2577	1514	2105	1787
108	2429	1377	1946	1659
114	2289	1245	1792	1539
120	2161	1121	1644	1424

based on time-averaged (initial time until the forecast time) large-scale diagnostics derived from global model analyses and static predictors derived from current storm conditions (e.g., DeMaria and Kaplan 1994a; DeMaria et al. 2005; Knaff et al. 2005). Best-track locations and intensities along with global analyses were used to create the developmental datasets, and these are referred to as the SHIPS developmental dataset hereafter. These data are described in CIRA (2016a).

A number of potential predictors were selected based on past research, as shown in Table 2. These include F_{R5} (SIZE), current intensity (VM), and 12-h intensity changes (PER). These three predictors are based solely on initial conditions and are referred to as static predictors. It is also known that storms tend to grow in terms of R5 as they intensify (K14). To better capture the potential intensification, potential intensity (PI) is included as a predictor. PI is defined by the SST-based empirical relationships of DeMaria and Kaplan (1994b)[2] and Whitney and Hobgood (1997)[3] in both the Atlantic and the Southern Hemisphere, and the East/central Pacific, respectively. PI in the WPAC is formulated as in the NATL, but the coefficients are $A = 19.7$ kt, $B = 88.0$ kt, and $C = 0.1909$. Relative humidity in the middle layers of the atmosphere (RH) is also purported to influence TC structure and size variations (e.g., Hill and Lackmann 2009; Xu and Wang 2010). Maclay et al. (2008) also showed how low-level temperature advection (TADV) and temperature gradients (TGR); vertical wind shear (VWS); trough interactions, which are related to relative eddy flux convergence (REFC); divergence at 200 hPa (D200); and sea surface temperature (SST) may play a role in TC in increasing the TC wind field (i.e., kinetic energy). Lee et al. (2010) showed how initial size (radial extent of 17 m s^{-1} wind speeds) and environmental relative vorticity (Z850) may also play a role in future size evolution (i.e., the idea of TC pedigree). Finally, it has long been known that latitude plays a role in TC size variations (Merrill 1984). This predictor set is similar to those used by Kozar and Misra (2014) to predict TC kinetic energy in the NATL.

As in the development of other statistical–dynamical models, we use a stepwise variable selection procedure where the 1% probabilities (based on an F test) were used for adding and removing variables at each step (see Wilks 2006, p. 210). Once the variables are selected for all lead times, a forward model is created that makes use of the complete set of those variables, mirroring the successful methodology used in SHIPS. All of the SHIPS developmental data were used to train regressions for our four separate TC basins. The regression equations will later be used to make a number of independent forecasts that will be discussed in the results section.

As a real-time application, these regression equations will predict $\Delta F_{R5}(t)$. Adding the initial F_{R5} (i.e., SIZE) to the forecast changes provides a forecast of $F_{R5}(t)$. To create forecasts of the TC size or R5(t), one multiplies $F_{R5}(t)$ by the intensity-based climatology of R5 (i.e., R5$_c$) using the forecast value of intensity at that time VM(t). For this study, VM(t)[4] comes from the decay-SHIPS forecast, which empirically decays the TC when it encounters land using the relationships described in DeMaria et al. (2006) and has implications for the predictive skill that will be discussed in the results section.

Summarizing, using the regression-based forecast of $\Delta F_{R5}(t)$ based on current conditions and forecast SHIPS diagnostics, as well as intensity forecasts VM (t), forecasts of the normalized TC size $F_{R5}(t)$, and more importantly TC size R5(t), are made. Recent work has shown how R5 and VM along with a storm motion vector can be used to estimate wind radii (Knaff et al. 2016, hereafter K16) using a vortex

[2] Here, PI(kt) = $A + Be^{C(30.0-SST)}$, where $A = 28.2$, $B = 55.8$, and $C = 0.1813$.

[3] Here, PI(kt) = $D + E$(SST), where $D = -79.17$ and $E = 5.361814$.

[4] Any VM(t) or position forecast could be used.

TABLE 2. Potential independent variables or predictors tested for their ability to predict the changes of the normalized TC size from the initial forecast time $\Delta F_{R5}(t)$. The basins where these predictors were selected are also provided.

Name	Description	Averaging area	Basin selected
SIZE	Initial normalized F_{R5}	—	All
VM	Current intensity	—	All
PER	12-h intensity trend	—	All
PI	Potential intensity	Same as SST	All
RH	Relative humidity (700–500 hPa)	200–800 km	All
TGR	Temp gradient (850–700 hPa) (from south to north)	0–500 km	All
D200	200-hPa divergence	0–1000 km	All
LAT	Sine of latitude	—	All
SST	Sea surface temp	At the TC center	All
REFC	Relative eddy flux convergence (Northern Hemisphere convention)	100–600 km	NATL, WPAC, SHEM
TADV	Temperature advection (850–700 hPa) (veering/backing Northern Hemisphere convention)	0–500 km	NATL, WPAC, SHEM
VWS	Vertical wind shear (200–850 hPa)	0–500 km	EPAC, WPAC, SHEM
Z850	Vorticity at 850 hPa	0–1000 km	WPAC, SHEM

model. This approach is also used here and is described next.

c. *Wind radii via a vortex model*

Given forecasts of R5(t), wind radii are then estimated using a vortex modeling approach, which was designed primarily for and is most valid for the purely tropical cyclone vortex (i.e., the vast majority of forecast cases). This procedure is illustrated in Fig. 3 using the observed R5 and best-track conditions for Hurricane Amanda at 0000 UTC 25 May. This is done by using a parametric model, namely the modified Rankine vortex (MRV), for each wind radii threshold (i.e., 34, 50, and 64 kt), where the azimuthally averaged wind field is a function of the intensity VM, radius r, and a shape parameter x. The MRV was chosen for its simplicity and its proven stability in the operational setting, its use in previous work (cf. Demuth et al. 2006, K07, and K16), and its ability to incorporate azimuthal wavenumber-1 asymmetries. To account for these asymmetries as a function of azimuth in terms of the angle measured from a direction 90° to the right (Northern Hemisphere) of the storm heading θ, parameters θ_o, the degree of rotation of the asymmetry from the direction 90° to the right of the storm motion vector, and the variable a,

Inputs	
Variable Names	**Values for Amanda (2014)**
TC size (R5)	11.02
Intensity (V_m)	90.00
Latitude (γ)	11.50
Storm Heading	297.00
Storm Speed (c)	4.40
Calculated	
Variable Names	**Values for Amanda (2014)**
R5 climatology ($R5_c$)	13.06
Normalized size (F_{R5})	0.84
Averaged R34	107.40
Averaged R50	55.90
Averaged R64	29.60
R_m (Climatology)	18.20
34-kt Bias correction	0.91
50-kt Bias correction	0.86
64-kt Bias correction	0.79
Asymmetry (a)	3.32
Phase (θ_o)	11.3
Output	
Variable Names	**Values for Amanda (2014)**
R34 (NE, SE, SW, NW)	120,105,95,120
R50 (NE, SE, SW, NW)	55, 50, 50, 55
R64 (NE, SE, SW, NW)	30,25,20,30

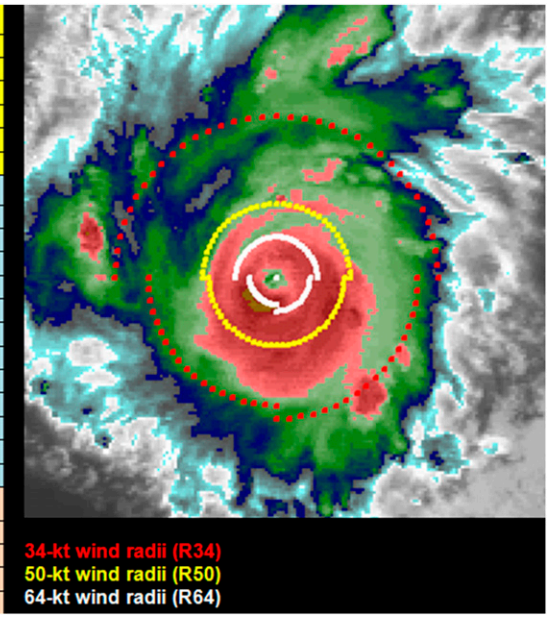

FIG. 3. (left) The inputs needed, values calculated, and resulting wind radii estimates based on the best track of Hurricane Amanda (2014) at 0000 UTC 25 May and (right) the corresponding IR image with the wind radii estimates overlaid.

TABLE 3. Variables used in the construction of the parametric vortex model presented in section 2c along with a brief description and physical interpretation (when needed).

Variable	Description	Physical interpretation
r	Radius	
θ	Azimuth, 90° to the right (Northern Hemisphere) of heading	Accounts for storm heading by placing the largest asymmetry to the right of motion (Northern Hemisphere)
θ_o	Degree of azimuthal rotation with respect to θ	Allows the asymmetry to move relative to its position determined by θ
a	Magnitude of the wavenumber-1 asymmetry	Determines the size of the wavenumber-1 asymmetry
VM	Max wind	Peak wind in the vortex
R_m	Radius of max winds	Location of max wind
R_{th}	Radius of a given threshold th	Azimuthally averaged wind radii
th	Wind radii threshold value	In this work, 34, 50, and 64 kt
B	Bias correction for the azimuthally averaged wind radii	Accounts for the use of nonzero wind radii to create azimuthally averaged R_{th}'s
x	Rankine vortex shape parameter	Determines the vortex shape or decay rate of the winds outside the radius of maximum winds
c	Vortex translations speed	Scalar of vortex motion
γ	Vortex latitude	
$V(r, \theta)$	Wind speed as a function of radius and azimuth in terms of θ	Note that for this application V is calculated for each available wind threshold th

defined as the magnitude of the asymmetry, are also required. The MRV equations used for this study are provided below. The MRV parameters are estimated from a combination of regression and climatology and closely follow the methodology discussed in K16. To further aid the reader, descriptions of the vortex model variables are also provided in Table 3:

$$V(r,\theta) = (\text{VM} - a)\left(\frac{r}{R_m}\right) + a\cos(\theta - \theta_o), \quad r < R_m \tag{3a}$$

and

$$V(r,\theta) = (\text{VM} - a)\left(\frac{R_m}{r}\right)^x + a\cos(\theta - \theta_o), \quad r \geq R_m. \tag{3b}$$

The first parameter estimated is the "shape parameter" x. It accounts for variations of the radial decay of the winds, with values close to 1.0 indicating very compact wind fields and small values (<0.3) indicating very broad wind fields. Estimating x is done for each wind radii threshold th. Two pieces of information are used to estimate x_{th}. The first is a climatological estimate of the radius of maximum wind R_m, which is a function of VM and the absolute value of latitude following Knaff et al. (2015). Nonzero azimuthally averaged wind radii estimates are based on regression equations detailed in K16 that are functions of R5 and VM. The use of nonzero azimuthally averaged wind radii results in high biases that increase when a storm has small wind radii with respect to the radius of maximum winds R_m. To account for the use of nonzero azimuthal averages in these regression equations, an additional empirically derived bias correction B is applied to each regression result as a function of distance between R_m and R_{th} and is given by

$$B = 0.0607\ln(R_{\text{th}} - R_m) + 0.6395, \quad (R_{\text{th}} - R_m) > 0. \tag{4}$$

The x_{th} values are then estimated [see Eq. (5) below]. Note that for this algorithm x_{th} are also constrained to fall between 0.1 and 1.0, where the latter value implies the vortex wind profile conserves angular momentum:

$$x_{\text{th}} = \log\left[\left(\frac{\text{th}}{\text{VM}}\right) \Big/ \left(\frac{R_m}{R_{\text{th}}}\right)\right]. \tag{5}$$

To account for the asymmetries as a function of azimuth θ, the degree of rotation of the asymmetry from the direction of 90° to the right of the storm motion vector θ_o and the magnitude of the asymmetry a, are required. To calculate a and θ_o, the climatological relationships developed for the North Atlantic version of DRCL (i.e., Table 1 in K07) are used. Those relationships represent the best fit that minimized the mean square differences between the observed wind radii and those calculated from the parametric model for a large sample[5] of cases found in the extended best track (Demuth et al. 2004) during 1988–2003 (see K07). The use of these climatological asymmetries as a function of

[5] In all, there were 8576, 6064, and 4320 radii of 34-, 50-, and 64-kt winds, respectively.

motion is justified by the results of both Uhlhorn et al. (2014) and Klotz and Jiang (2016), who showed that surface azimuthal wind asymmetries are to first order as a result of translation. The storm motion vector is calculated from the track forecasts associated with the decay-SHIPS intensity forecast. In this formulation,

$$a = 1.06 + 0.28c - 0.0026c^2 - 0.08(|\gamma| - 25) \quad \text{and} \quad (6)$$

$$\theta_o = 17.0 + 0.08(|\gamma| - 25) - 1.05c, \quad (7)$$

where c is the storm speed (kt) and γ is the latitude. The same values of a and θ_o are used for each wind speed threshold. Note that for SHEM TCs the asymmetries are a mirror image of those of the Northern Hemisphere.

Using the parameters VM, R_m, a, θ_o, and θ (i.e., perpendicular to the provided motion vector); x_{34}, x_{50}, and x_{64}; and the MRV equations [Eqs. (3a) and (3b)], complete vortices for each wind threshold (i.e., V_{34}, V_{50}, and V_{64}) are constructed for each forecast time. The value of VM(t) determines which vortex equations are used. For instance, if VM(t) is 60 kt at $t = 48$ h, only V_{34} and V_{50} are constructed at the 48-h forecast time. By searching through each azimuth (16 azimuthal directions in this case), the maximum extent of each wind threshold in each earth-relative quadrant is found. In this manner the traditional wind radii can be estimated. Again, Fig. 3 illustrates the steps taken to estimate wind radii given inputs based on the best track and satellite imagery, and Table 3 provides the variables used along with their description. While this description seems complicated, it is generally less involved, especially in terms of programming and maintenance, than trying to predict wind radii in individual quadrants. This vortex model approach also ensures results that are consistent with the intensity forecast VM(t).

d. Validating wind radii

Forecast values of 34-, 50-, and 64-kt wind radii in each quadrant and at each forecast lead time are compared with the final best-track values in the NATL and EPAC to validate forecasts. At present, the WPAC and SHEM wind radii are not best tracked[6] following the season, and forecasts in those basins will not be validated. The occurrence of zero-valued wind radii introduces an added complication when verifying wind radii. The zero-valued wind radii typically occur when storms are near the wind radii threshold intensity or when storms are translating rapidly. For this study, the verification strategy follows that of Sampson and Knaff (2015), as follows. If any of the quadrants in the best track have nonzero wind radii, all quadrants for that case are tested. This strategy allows the individual quadrant statistics to be combined to form a single measurement of mean absolute error and bias for each forecast lead time.

For comparison, the validation of the vortex model presented in section 2c, with the bias correction, produced 34-kt wind radii mean absolute errors of 25 and 33 n mi and biases of 11 and −11 n mi, based on 2 yr (2014–15) of scatterometry imagery in the NATL and EPAC (243 cases) and a wind radii best track for the WPAC (3138 cases), as reported in Sampson et al. (2017). These validations were performed for all cases, including TCs transitioning to an extratropical structure or those that had an extratropical structure that were contained in the best track. Our results are based the same approach.

3. Results

a. Selected variables and interpretation

The stepwise multiple regression procedure selected 11, 10, 13, and 12 predictors for the NATL, EPAC, WPAC, and SHEM basins from the list of potential predictors in Table 2. In the NATL, the predictors Z850 and VWS were not selected in the procedure. In the EPAC, on the other hand, the TADV, REFC, and Z850 predictors were not selected. In the SHEM, only the PI predictor was not selected and in the WPAC all the potential predictors were selected. To help the reader, Table 2 also lists the basins in which each potential predictor is used. The lack of statistical importance of Z850 as a predictor in the NATL and EPAC likely indicates that most TCs are moving in a trade wind environment for most of their life cycles in those basins. In a similar manner, the statistical unimportance of TADV and REFC in the EPAC may also reflect the infrequent encounters of TCs with strong atmospheric temperature gradients and troughs.

The normalized regression coefficients for the PI, SST, and VM terms are large and sometimes indicate relationships that are opposite of physical reasoning. Such behavior in multiple regressions often signals that the linear model is trying to accommodate a nonlinear behavior. To examine the underlying relationships, ΔF_{R5} as a function of SST and VM at a lead time of 48 h is plotted, while holding the other variables fixed (Fig. 4). TC growth in each basin behaves quite differently in the SST and VM parameter space. The NATL panel indicates that all TCs in the NATL tend to grow over the entire SST and VM space, with the largest

[6] Wind radii values are provided in the best-track records provided by JTWC, but those represent the values that were used in real time and are not revisited after the season.

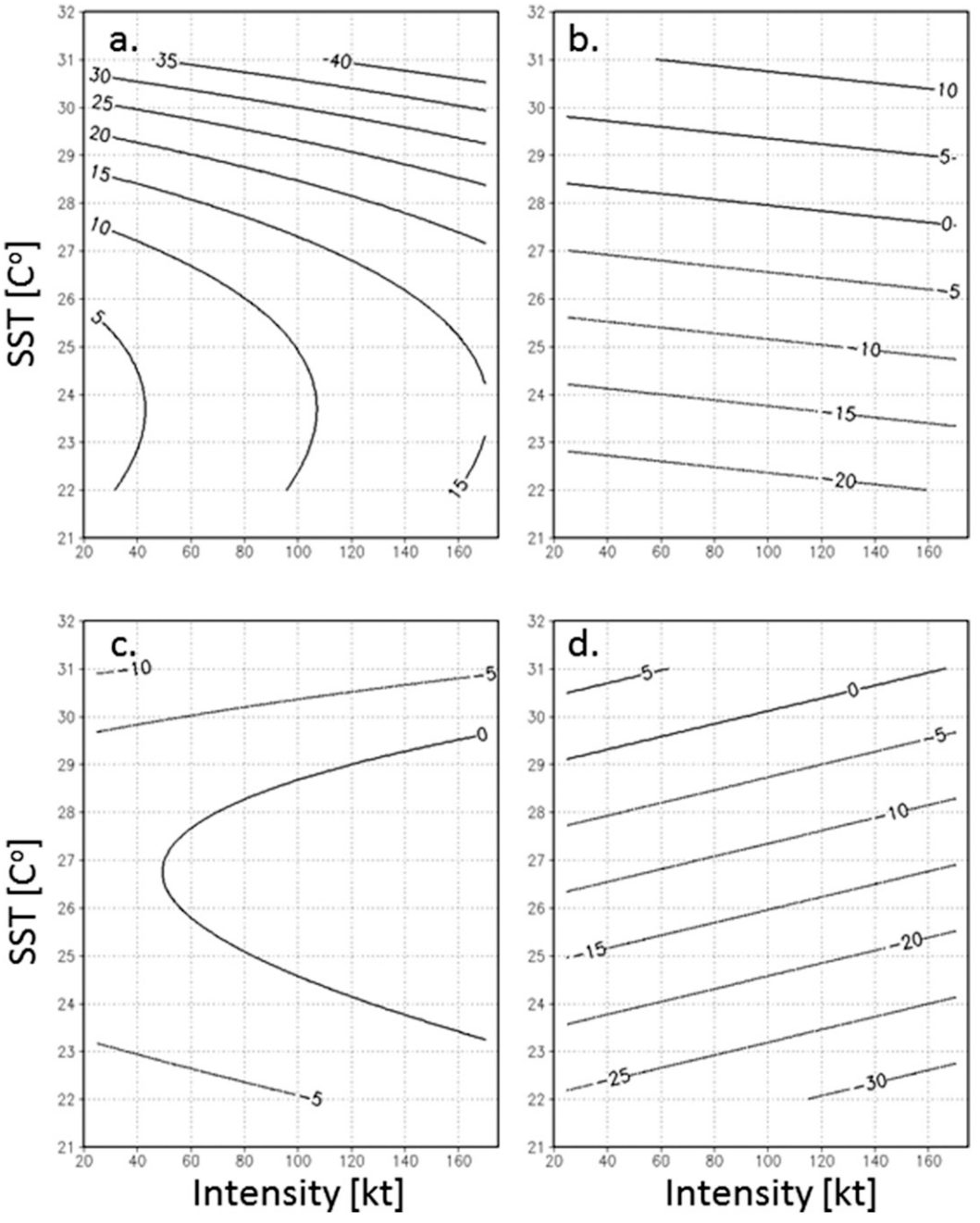

FIG. 4. The 48-h combined SST and VM relationship to ΔF_{R5} in the (a) NATL, (b) EPAC, (c) WPAC, and (d) SHEM. The contoured field is ΔF_{R5}.

growth occurring for TCs in very warm SST environments. In the EPAC, growth again generally occurs in the warmest SSTs (i.e., >28.5°C), but below that SST TCs tend to shrink. In contrast, the WPAC TCs seem to grow only slightly in a relatively narrow range of moderate SSTs and only at the highest intensities. This may indicate growth during rather intense TC weakening as they encounter progressively cooler SST conditions. In the SHEM, weaker TCs appear to prefer growth over quite warm SSTs (>29°C), but TCs generally shrink in cooler SST conditions. Plots from other lead times are similar to those shown in Fig. 4.

To examine the strength and signs of the remaining relationships in the multiple regression equations, Fig. 5 shows the normalized regression coefficients for the remaining predictor set at 24, 48, 72, 96, and 120 h and in

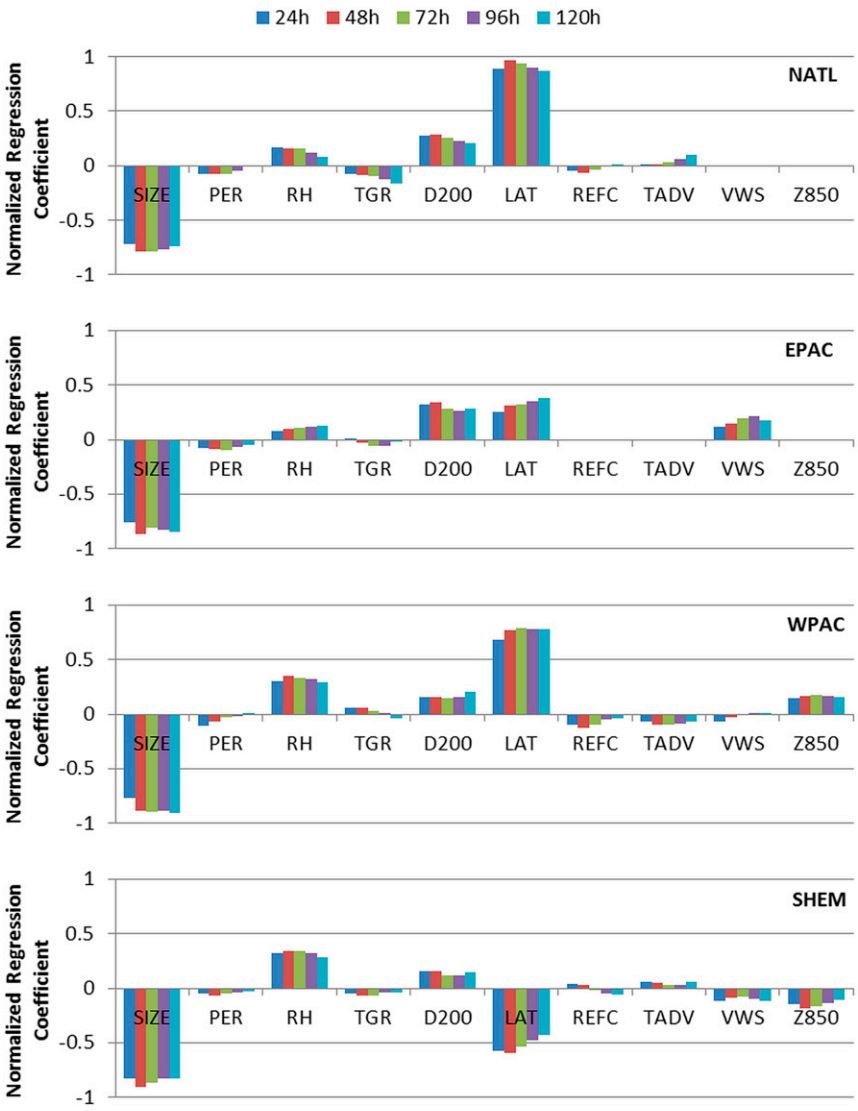

FIG. 5. Plots of normalized regression coefficients for the multiple regressions that forecast ΔF_{R5}. These are displayed for the NATL, EPAC, WPAC, and SHEM and at forecast lead times of 24, 48, 72, 96, and 120 h.

all basins. The strongest and most consistent relationships are between the SIZE, LAT, D200, and RH. The signs of these relationships suggest that storms that are large (small) relative to the mean SIZE tend to shrink (grow). The regressions also suggest that greater than average D200 and RH also promote growth of TCs. The latter (higher RH promotes growth) is consistent with previous modeling results, such as those of Hill and Lackmann (2009) and Xu and Wang (2010). Less interesting is the finding that higher LAT is also related to TC growth, which has long been known (i.e., Merrill 1984).

Predictors with less pronounced forecast influence include PER, TGR, REFC, TADV, VWS, and Z850. Intensification (i.e., positive PER) promotes the slight shrinking of TCs in all basins. Similarly, positive (Northern Hemisphere) REFC, as it promotes vortex intensification when other factors are held constant or favorable (e.g., Molinari and Vollaro 1989, 1990; DeMaria et al. 1993; Leroux et al. 2016, and additional references therein), also promotes a reduction in storm sizes. Positive Z850 (Northern Hemisphere) appears to be related to TC growth in the SHEM and WPAC where TCs often form in monsoon trough environments (equatorial westerlies converging with poleward easterlies). This is likely due to imports of low-level angular momentum in monsoon trough environments consistent with the findings of Chan and Chan (2013, 2015). Positive TADV

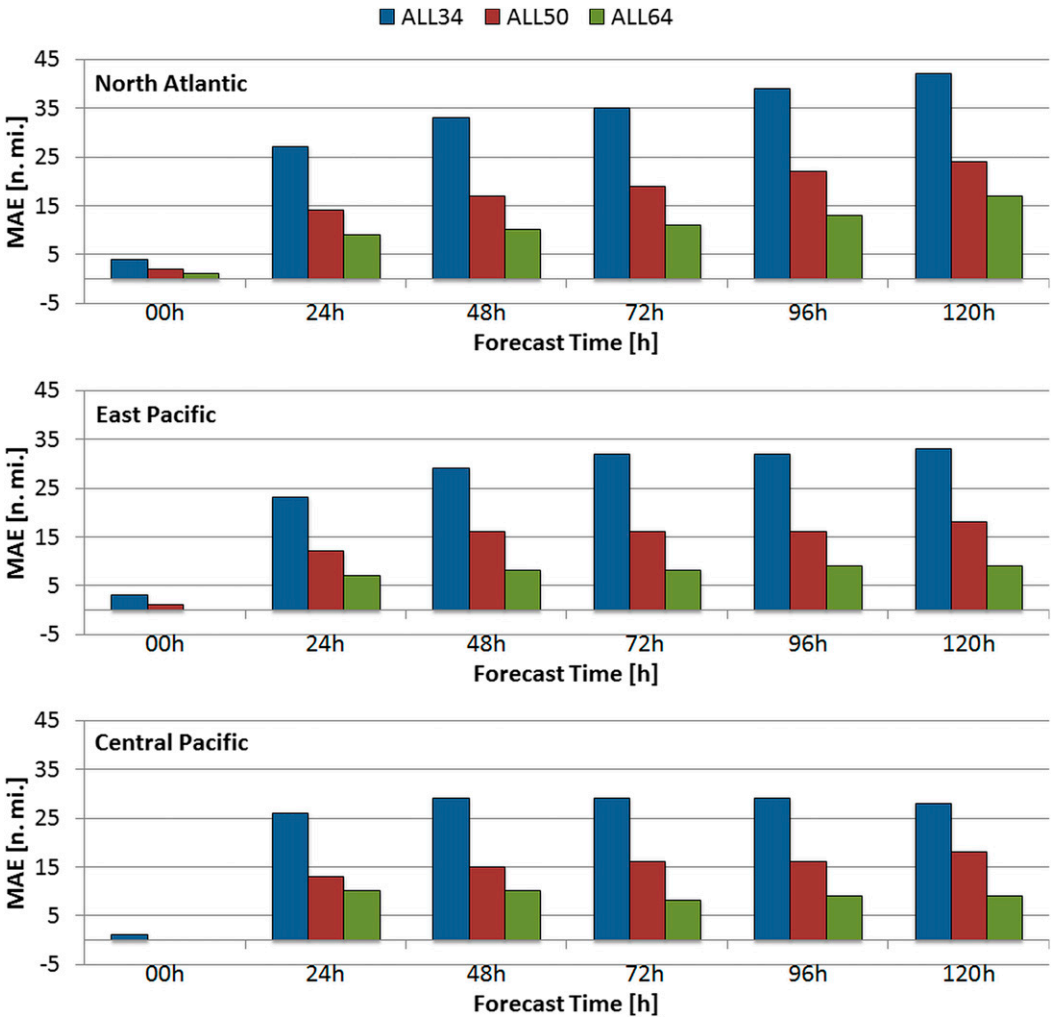

FIG. 6. MAEs associated with independent wind radii forecasts during the 2014 and 2015 hurricane seasons. The statistics of the four geographic quadrants have been combined. Results are shown for storms developing in the NATL, the east Pacific (east of 140°W) and the central Pacific (between 180° and 140°W).

(Northern Hemisphere convention) is generally associated with TC growth and is consistent with the findings of Maclay et al. (2008). The remaining terms TGR and VWS seem to have more variable interpretations. Alone, increased VWS and TGR are related to growth, but the increased TGR is also related to zonal wind shear, which complicates the interpretation.

b. *Independent performance*

To assess the performance of these wind radii forecasts, the 2014 and 2015 seasons are reforecast in the NATL and EPAC. Reforecasts are based on real-time NHC advisories, decay-SHIPS intensity, track, and large-scale diagnostics. These diagnostics were created in real time at NHC and are based on the available real-time Global Forecast System (GFS) forecasts. IR-based TC size estimates were calculated after the fact, but using the real-time advisory information. Thus, the reforecasts simulate nearly identically a system that was run in real time, save for small (0.5 h) differences in IR image availability. These decay-SHIPS-based wind radii (DSWR) forecasts are also independent of the developmental dataset.

Figures 6 and 7 shows the mean absolute error (MAE) and bias statistics in the NATL and EPAC. For simplicity, a single measure for the MAE/bias is shown where the performance of the geographic quadrants is combined. The EPAC is further broken down to storms forming in the central Pacific (140°W–180°) and east Pacific (east of 140°W), as different organizations construct the best tracks of these storms. The statistical significance of these results versus other forecasts or a baseline is difficult to assess because of the numbers of cases (Table 4) and the strong serial correlations

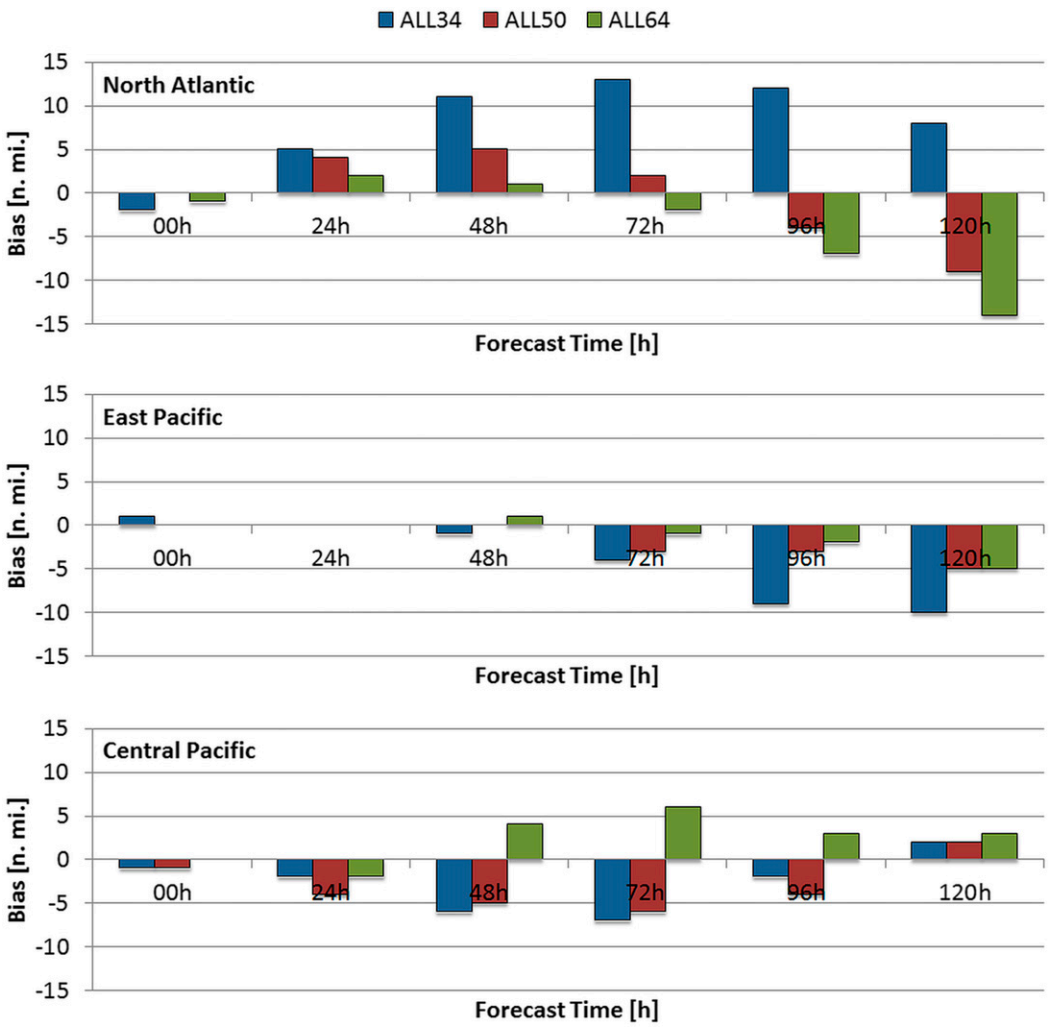

FIG. 7. As in Fig. 6, but showing forecast biases.

between adjacent times. Results indicate that MAEs are typically less than 30, 20, and 10 n mi for the 34-, 50-, and 64-kt wind radii forecasts, respectively. These are rather respectable results given the vortex model's capabilities discussed in section 3d. The biases are negative in the EPAC basins and straddle zero in the NATL. The biases appear to be somewhat related to decay-SHIPS intensity errors that were slightly negative to near zero in the Atlantic and slightly negative to distinctly negative (less than −5 kt) in the east Pacific, with negative biases in the central Pacific during these two seasons (Cangialosi and Franklin 2015, 2016). Note the vortex model's positive biases in these basins versus scatterometry fixes.

Overall, our results suggest that these forecasts are competitive with forecasts made by regional hurricane forecast models and the DRCL (K07) used for skill analysis (see Figs. 4 and 5 in Sampson and Knaff 2015). One benefit of the DSWR is that its forecasts are relatively independent of other forecasts[7] and that adding them to a wind radii forecast consensus (cf. Sampson and Knaff 2015) generally reduces the consensus 34-, 50-, and 64-kt wind radii forecast errors. In fact, these decay-SHIPS-based forecasts result in no degradation or reductions of consensus errors (on the order of 0–1 n mi) and reduction of negative biases based on a 2014–15 EPAC and NATL sample. For instance, 34-kt wind radii forecasts are improved by 1, 1, 0, 1, and 0 n mi with bias reductions of 1, 1, 1, 1, and 1 n mi at 12-, 24-, 36-, 48-, and 72-h lead times. These reductions of about 1 n mi are also found for 50- and 64-kt wind radii

[7] This concept of consensus member independence and consensus improvement is described in the appendixes in Sampson et al. (2008).

TABLE 4. The numbers of TC forecast cases and estimated independent cases (in parentheses) available for the statistics shown in Figs. 6 and 7 are listed. The number of independent cases or degrees of freedom is based upon an assumed 30-h serial correlation.

	0 h	24 h	48 h	72 h	96 h	120 h
			North Atlantic			
34 kt	208 (65)	161 (52)	120 (39)	82 (26)	50 (18)	26 (11)
50 kt	105 (34)	88 (28)	74 (23)	59 (17)	36 (11)	23 (9)
64 kt	72 (23)	50 (18)	43 (15)	39 (14)	23 (9)	15 (6)
			East Pacific			
34 kt	682 (184)	610 (258)	501 (129)	395 (103)	289 (79)	207 (58)
50 kt	457 (125)	413 (112)	344 (92)	260 (71)	174 (49)	106 (32)
64 kt	312 (92)	257 (71)	222 (61)	156 (47)	89 (27)	60 (18)
			Central Pacific			
34 kt	79 (23)	70 (20)	69 (21)	61 (17)	56 (15)	51 (13)
50 kt	37 (13)	35 (11)	38 (12)	41 (13)	41 (12)	40 (10)
64 kt	18 (7)	17 (7)	20 (5)	25 (6)	25 (6)	23 (5)

thresholds, with the majority of the error reduction coming from improved biases.

c. *Example forecasts*

Two forecasts are now presented to give the reader an idea of what representative forecasts look like and how they compare to the corresponding best tracks. We have purposely chosen cases in which track and intensity forecasts were close, yet not identical, to the verification so that we could more confidently discuss predicted changes in the wind radii unrelated to those predictors while still highlighting the dependencies of wind radii on the forecast track and intensity.

Figure 8 shows the DSWR forecasts of Hurricanes Edouard (al062014) and Linda (ep152015) and the corresponding best tracks. To improve readability, only the 34- and 64-kt wind radii are shown for these cases. The 0000 UTC 12 September DSWR forecast and corresponding best track are shown for Edouard (Fig. 8, top two panels). During the 5-day forecast, Edouard intensified and recurved. During the intensification period, the wind radii expanded. A similar pattern of behavior is seen in the DSWR forecast, but the wind radii are handicapped by the underforecast of intensity and a track forecast that does not indicate recurvature. Similarly, early in the Edouard forecast the intensity forecasts were too high, leading to slightly larger 34-kt wind radii in the northeast quadrants. The bottom two panels in Fig. 8 show the 0000 UTC 8 September forecast for Linda and the corresponding best track. In this case, the track forecast was nearly perfect and the majority of the errors (and low bias) appear to be related to the underforecast of intensity, though at the end of the forecast period the DRWR forecast would likely have been too big even with a perfect intensity forecast. The DSWR-predicted wind radii asymmetries are very similar to the best-track wind radii asymmetries. In both forecast cases shown here, the DSWR captures many aspects of the wind radii evolution, but these individual forecasts also show some of the dependence of the wind radii to both the intensity and the track forecast used in the decay-SHIPS model.

4. Summary, discussion, and future work

This paper has detailed a statistical–dynamical method for forecasting wind radii using decay-SHIPS intensity and track forecasts, associated large-scale GFS-forecast-based diagnostic files, and information derived from current IR imagery and TC advisories. The independent variable predicted is the change from $t = 0$ of the normalized (by intensity) IR-based TC size or R5 (see K14). The estimation of the wind radii is done parametrically using the method of K16 and utilizing the decay-SHIPS track and intensity forecast along with the predicted changes in the IR-based TC size R5. The method produces stable forecasts of wind radii that are competitive with the current operational methods. Furthermore, the addition of these independent forecasts into wind radii consensus forecasts (Sampson and Knaff 2015) suggests that the forecasts provide independent information that reduces forecast errors and bias among the consensus forecasts at most forecast lead times and all wind radii.

This model has been developed for the majority of tropical cyclone basins. Here, we compare to the NHC-based best tracks of wind radii in the NATL and EPAC, as such validation datasets do not yet exist in the WPAC or SHEM. The model is currently running and making forecasts for all of these basins at the Cooperative Institute for Research in the Atmosphere. The forecasts in the NATL and EPAC are also being tested by the Joint Hurricane Testbed and should be soon incorporated

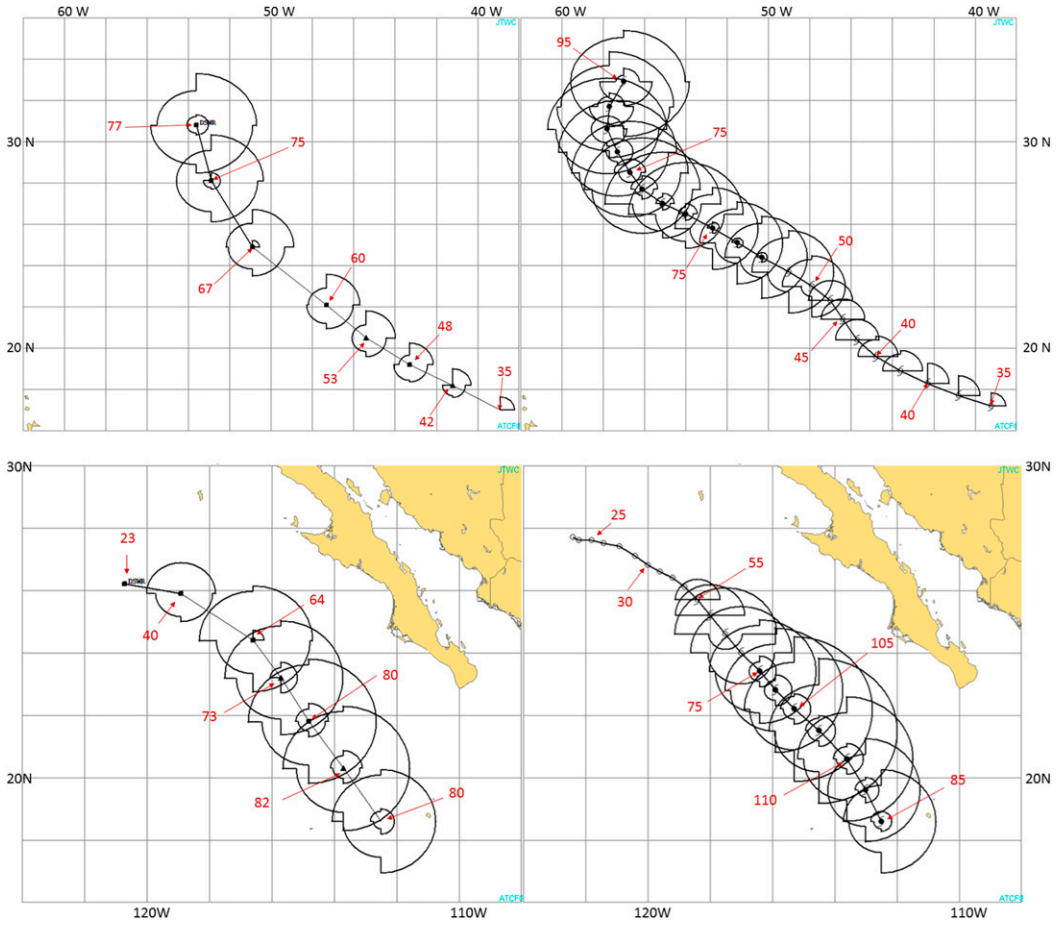

FIG. 8. (left) DSWR forecasts for Hurricanes (top) Edouard (0000 UTC 12 Sep 2014) and (bottom) Linda (0000 UTC 8 Sep 2015) with (right) corresponding best tracks. To improve the esthetics and readability of the figures, only the 34- and 64-kt wind radii are shown, the latter being shown as inner concentric rings when the intensity exceeds 64 kt. Note how intensity biases affect the forecast of wind radii with under- (over-) forecasts of intensity corresponding to slightly smaller (larger) 34-kt wind radii.

into the real-time experimental processing in the operational computing environment at NHC. In the very near future, these methods should also be transitioned to the Automated Tropical Cyclone Forecast System (ATCF; Sampson and Schrader 2000) and operations at the JTWC, where they will become part of the wind radii consensus forecast. It is here that this capability may be most important as it is expected that this consensus capability should dramatically improve JTWC's wind radii estimates and forecasts, which will provide improved input to several operational products including wind speed probabilities (DeMaria et al. 2009, 2013), wave forecasts (Sampson et al. 2010, 2013, 2016), model initialization (e.g., Trahan and Sparling 2012), and improved objectively determined Department of Defense TC conditions of readiness (Sampson et al. 2012).

Since all the information needed to estimate the minimum sea level pressure (MSLP) using the wind–pressure relationship (WPR) of Courtney and Knaff (2009) is available, forecast values of MSLP(t) that are consistent with decay-SHIPS intensity, track, and wind radii forecasts are created and provided with the wind radii forecasts. This WPR explicitly accounts for MSLP variations as a function of VM, storm latitude, 34-kt wind radii, and storm translation speed, and should produce physically consistent MSLP forecasts. This WPR is also used at NHC, JTWC, and the Australian tropical cyclone warning centers (Perth, Western Australia; Darwin, Northern Territory; and Brisbane, Queensland) to determine MSLPs operationally. The addition of MSLP estimates is provided and will be validated/evaluated in the future. It is also recognized that MSLP is not forecast by NHC nor JTWC. However, some WMO regional meteorological specialized centers make MSLP forecasts, noting that many of the regional specialized meteorological centers (RSMCs) routinely

receive JTWC's guidance products. MSLP estimates are also useful for other TC risk applications like storm surge and risk models that use pressure-based vortex parameterizations [e.g., the Holland (1980) model].

Before being employed in operations, the coefficients will be updated to use a longer developmental dataset, noting that we left out 2 yr here to test the scheme with independent data. Finally, the vortex model used in this work uses climatological motion-relative asymmetries. These asymmetries can likely be improved by 1) incorporating known causes of convective and wind field asymmetries into this methodology and 2) specifically addressing the extratropical transitioning and extratropical stages of TCs. That work will be the focus of future studies.

Acknowledgments. This basis for this work, encompassing many years, has been supported by NOAA/NESDIS base funding and numerous NOAA programs including the Geostationary Operational Environmental Satellite (GOES) Improved Measurement and Product Assurance Plan (GIMPAP), the GOES-R Risk Reduction (GOESR3) project, and the Joint Hurricane Testbed (JHT) under NOAA Grant NA17RJ1228 at the Cooperative Institute for Research in the Atmosphere at Colorado State University. The GIMPAP and GOESR3 programs were supported by the GOES Program Office. JHT research is fully supported by the U.S. Weather Research Program in NOAA/OAR's Office of Weather and Air Quality. The continued support of tropical cyclone research provided by the Office of Naval Research and the advocacy of the U.S. Navy is also sincerely appreciated. We also acknowledge the assistance of Jack Dostalek and Chris Slocum, who provided comments on previous versions of this manuscript. Finally, we thank the three anonymous reviewers who provided many constructive suggestions. The views, opinions, and findings contained in this report are those of the authors and should not be construed as an official National Oceanic and Atmospheric Administration or U.S. government position, policy, or decision.

REFERENCES

Bender, M. A., I. Ginis, R. Tuleya, B. Thomas, and T. Marchok, 2007: The operational GFDL coupled hurricane–ocean prediction system and a summary of its performance. *Mon. Wea. Rev.*, **135**, 3965–3989, doi:10.1175/2007MWR2032.1.

Bernardet, L., and Coauthors, 2015: Community support and transition of research to operations for the Hurricane Weather Research and Forecast Model (HWRF). *Bull. Amer. Meteor. Soc.*, **96**, 953–960, doi:10.1175/BAMS-D-13-00093.1.

Cangialosi, J. P., and J. L. Franklin, 2015: 2014 National Hurricane Center Forecast verification report. NOAA/National Hurricane Center, 82 pp. [Available online at http://www.nhc.noaa.gov/verification/pdfs/Verification_2014.pdf.]

——, and ——, 2016: 2015 National Hurricane Center Forecast verification report. NOAA/National Hurricane Center, 69 pp. [Available online at http://www.nhc.noaa.gov/verification/pdfs/Verification_2015.pdf.]

——, and C. W. Landsea, 2016: An examination of model and official National Hurricane Center tropical cyclone size forecasts. *Wea. Forecasting*, **31**, 1293–1300, doi:10.1175/WAF-D-15-0158.1.

Carter, G. M., J. P. Dallavalle, and H. R. Glahn, 1989: Statistical forecasts based on the National Meteorological Center's numerical weather prediction system. *Wea. Forecasting*, **4**, 401–412, doi:10.1175/1520-0434(1989)004<0401:SFBOTN>2.0.CO;2.

Chan, K. T. F., and J. C. L. Chan, 2013: Angular momentum transports and synoptic flow patterns associated with tropical cyclone size change. *Mon. Wea. Rev.*, **141**, 3985–4007, doi:10.1175/MWR-D-12-00204.1.

——, and ——, 2015: Impacts of vortex intensity and outer winds on tropical cyclone size. *Quart. J. Roy. Meteor. Soc.*, **141**, 525–537, doi:10.1002/qj.2374.

CIRA, 2016a: SHIPS developmental data. Cooperative Institute for Research in the Atmosphere. [Available online at http://rammb.cira.colostate.edu/research/tropical_cyclones/ships/developmental_data.asp.]

——, 2016b: TC track model guidance used by NHC. Cooperative Institute for Research in the Atmosphere. [Available online at http://rammb.cira.colostate.edu/training/visit/training_sessions/tc_track_model_guidance_used_by_nhc/.]

Courtney, J., and J. A. Knaff, 2009: Adapting the Knaff and Zehr wind–pressure relationship for operational use in tropical cyclone warning centres. *Aust. Meteor. Oceanogr. J.*, **58**, 167–179.

DeMaria, M., 2009: A simplified dynamical system for tropical cyclone intensity prediction. *Mon. Wea. Rev.*, **137**, 68–82, doi:10.1175/2008MWR2513.1.

——, and J. Kaplan, 1994a: A statistical hurricane intensity prediction scheme (SHIPS) for the Atlantic basin. *Wea. Forecasting*, **9**, 209–220, doi:10.1175/1520-0434(1994)009<0209:ASHIPS>2.0.CO;2.

——, and ——, 1994b: Sea surface temperature and the maximum intensity of Atlantic tropical cyclones. *J. Climate*, **7**, 1324–1334, doi:10.1175/1520-0442(1994)007<1324:SSTATM>2.0.CO;2.

——, ——, and J.-J. Baik, 1993: Upper-level eddy angular momentum fluxes and tropical cyclone intensity change. *J. Atmos. Sci.*, **50**, 1133–1147, doi:10.1175/1520-0469(1993)050<1133:ULEAMF>2.0.CO;2.

——, M. Mainelli, L. K. Shay, J. A. Knaff, and J. Kaplan, 2005: Further improvement to the Statistical Hurricane Intensity Prediction Scheme (SHIPS). *Wea. Forecasting*, **20**, 531–543, doi:10.1175/WAF862.1.

——, J. A. Knaff, and J. Kaplan, 2006: On the decay of tropical cyclone winds crossing narrow landmasses. *J. Appl. Meteor.*, **45**, 491–499, doi:10.1175/JAM2351.1.

——, ——, and C. R. Sampson, 2007: Evaluation of long-term trend in tropical cyclone intensity forecasts. *Meteor. Atmos. Phys.*, **97**, 19–28, doi:10.1007/s00703-006-0241-4.

——, ——, R. Knabb, C. Lauer, C. R. Sampson, and R. T. DeMaria, 2009: A new method for estimating tropical cyclone wind speed probabilities. *Wea. Forecasting*, **24**, 1573–1591, doi:10.1175/2009WAF2222286.1.

——, and Coauthors, 2013: Improvements to the operational tropical cyclone wind speed probability model. *Wea. Forecasting*, **28**, 586–602, doi:10.1175/WAF-D-12-00116.1.

——, C. R. Sampson, J. A. Knaff, and K. D. Musgrave, 2014: Is tropical cyclone intensity guidance improving? *Bull. Amer. Meteor. Soc.*, **95**, 387–398, doi:10.1175/BAMS-D-12-00240.1.

Demuth, J. L., M. DeMaria, J. A. Knaff, and T. H. Vonder Haar, 2004: Evaluation of Advanced Microwave Sounding Unit tropical-cyclone intensity and size estimation algorithms. *J. Appl. Meteor.*, **43**, 282–296, doi:10.1175/1520-0450(2004)043<0282:EOAMSU>2.0.CO;2.

——, ——, and ——, 2006: Improvement of Advanced Microwave Sounding Unit tropical cyclone intensity and size estimation algorithms. *J. Appl. Meteor. Climatol.*, **45**, 1573–1581, doi:10.1175/JAM2429.1.

Dolling, K., E. Ritchie, and J. Tyo, 2016: The use of the deviation angle variance technique on geostationary satellite imagery to estimate tropical cyclone size parameters. *Wea. Forecasting*, **31**, 1625–1642, doi:10.1175/WAF-D-16-0056.1.

Hill, K. A., and G. M. Lackmann, 2009: Influence of environmental humidity on tropical cyclone size. *Mon. Wea. Rev.*, **137**, 3294–3315, doi:10.1175/2009MWR2679.1.

Holland, G. J., 1980: An analytic model of the wind and pressure profiles in hurricanes. *Mon. Wea. Rev.*, **108**, 1212–1218, doi:10.1175/1520-0493(1980)108<1212:AAMOTW>2.0.CO;2.

Klotz, B. W., and H. Jiang, 2016: Global composites of surface wind speeds in tropical cyclones based on a 12 year scatterometer database. *Geophys. Res. Lett.*, **43**, 10 480–10 488, doi:10.1002/2016GL071066.

Knaff, J. A., and B. A. Harper, 2010: Tropical cyclone surface wind structure and wind-pressure relationships. *Proc. Int. Workshop on Tropical Cyclones—VII*, La Reunion, France, WMO, KN1. [Available online at http://www.wmo.int/pages/prog/arep/wwrp/tmr/otherfileformats/documents/KN1.pdf.]

——, and C. R. Sampson, 2015: After a decade are Atlantic tropical cyclone gale force wind radii forecasts now skillful? *Wea. Forecasting*, **30**, 702–709, doi:10.1175/WAF-D-14-00149.1.

——, M. DeMaria, C. R. Sampson, and J. M. Gross, 2003: Statistical, 5-day tropical cyclone intensity forecasts derived from climatology and persistence. *Wea. Forecasting*, **18**, 80–92, doi:10.1175/1520-0434(2003)018<0080:SDTCIF>2.0.CO;2.

——, C. R. Sampson, and M. DeMaria, 2005: An operational statistical typhoon intensity prediction scheme for the western North Pacific. *Wea. Forecasting*, **20**, 688–699, doi:10.1175/WAF863.1.

——, C. Guard, J. Kossin, T. Marchok, C. Sampson, T. Smith, and N. Surgi, 2006: Operational guidance and skill in forecasting structure change. *Proc. Int. Workshop on Tropical Cyclones—VI*, San Juan, Costa Rica, WMO, 160–184. [Available online at http://severe.worldweather.org/iwtc/document/Topic_1_5_John_Knaff.pdf.]

——, C. R. Sampson, M. DeMaria, T. P. Marchok, J. M. Gross, and C. J. McAdie, 2007: Statistical tropical cyclone wind radii prediction using climatology and persistence. *Wea. Forecasting*, **22**, 781–791, doi:10.1175/WAF1026.1.

——, M. DeMaria, S. P. Longmore, and R. T. DeMaria, 2014a: Improving tropical cyclone guidance tools by accounting for variations in size. *31st Conf. on Hurricanes and Tropical Meteorology*, San Diego, CA, Amer. Meteor. Soc., 51. [Available online at https://ams.confex.com/ams/31Hurr/webprogram/Paper244165.html.]

——, S. P. Longmore, and D. A. Molenar, 2014b: An objective satellite-based tropical cyclone size climatology. *J. Climate*, **27**, 455–476, doi:10.1175/JCLI-D-13-00096.1.

——, ——, R. T DeMaria, and D. A. Molenar, 2015: Improved tropical cyclone flight-level wind estimates using routine infrared satellite reconnaissance. *J. Appl. Meteor. Climatol.*, **54**, 463–478, doi:10.1175/JAMC-D-14-0112.1.

——, C. J. Slocum, K. D. Musgrave, C. R. Sampson, and B. Strahl, 2016: Using routinely available information to estimate tropical cyclone wind structure. *Mon. Wea. Rev.*, **144**, 1233–1247, doi:10.1175/MWR-D-15-0267.1.

Kossin, J. P., J. A. Knaff, H. I. Berger, D. C. Herndon, T. A. Cram, C. S. Velden, R. J. Murnane, and J. D. Hawkins, 2007: Estimating hurricane wind structure in the absence of aircraft reconnaissance. *Wea. Forecasting*, **22**, 89–101, doi:10.1175/WAF985.1.

Kozar, M. E., and V. Misra, 2014: Statistical prediction of integrated kinetic energy in North Atlantic tropical cyclones. *Mon. Wea. Rev.*, **142**, 4646–4657, doi:10.1175/MWR-D-14-00117.1.

Landsea, C. W., and J. L. Franklin, 2013: Atlantic hurricane database uncertainty and presentation of a new database format. *Mon. Wea. Rev.*, **141**, 3576–3592, doi:10.1175/MWR-D-12-00254.1.

Lee, C. S., K. K. W. Cheung, W.-T. Fang, and R. L. Elsberry, 2010: Initial maintenance of tropical cyclone size in the western North Pacific. *Mon. Wea. Rev.*, **138**, 3207–3223, doi:10.1175/2010MWR3023.1.

Leroux, M.-D., M. Plu, and F. Roux, 2016: On the sensitivity of tropical cyclone intensification under upper-level trough forcing. *Mon. Wea. Rev.*, **144**, 1179–1202, doi:10.1175/MWR-D-15-0224.1.

Maclay, K. S., M. DeMaria, and T. H. Vonder Haar, 2008: Tropical cyclone inner-core kinetic energy evolution. *Mon. Wea. Rev.*, **136**, 4882–4898, doi:10.1175/2008MWR2268.1.

Marchok, T. P., 2002: How the NCEP tropical cyclone tracker works. Preprints, *25th Conf. on Hurricanes and Tropical Meteorology*, San Diego, CA, Amer. Meteor. Soc., 21–22. [Available online at https://ams.confex.com/ams/pdfpapers/37628.pdf.]

Merrill, R. T., 1984: A comparison of large and small tropical cyclones. *Mon. Wea. Rev.*, **112**, 1408–1418, doi:10.1175/1520-0493(1984)112<1408:ACOLAS>2.0.CO;2.

Molinari, J., and D. Vollaro, 1989: External influences on hurricane intensity. Part I: Outflow layer eddy momentum fluxes. *J. Atmos. Sci.*, **46**, 1093–1105, doi:10.1175/1520-0469(1989)046<1093:EIOHIP>2.0.CO;2.

——, and ——, 1990: External influences on hurricane intensity. Part II: Vertical structure and response of the hurricane vortex. *J. Atmos. Sci.*, **47**, 1902–1918, doi:10.1175/1520-0469(1990)047<1902:EIOHIP>2.0.CO;2.

Mueller, K. J., M. DeMaria, J. A. Knaff, J. P. Kossin, and T. H. Vonder Haar, 2006: Objective estimation of tropical cyclone wind structure from infrared satellite data. *Wea. Forecasting*, **21**, 990–1005, doi:10.1175/WAF955.1.

NHC, 2009: NHC track and intensity models. National Hurricane Center. [Available online at http://www.nhc.noaa.gov/modelsummary.shtml.]

Rappaport, E. N., and Coauthors, 2009: Advances and challenges at the National Hurricane Center. *Wea. Forecasting*, **24**, 395–419, doi:10.1175/2008WAF2222128.1.

Sampson, C. R., and A. J. Schrader, 2000: The Automated Tropical Cyclone Forecasting System (version 3.2). *Bull. Amer. Meteor. Soc.*, **81**, 1231–1240, doi:10.1175/1520-0477(2000)081<1231:TATCFS>2.3.CO;2.

——, and J. A. Knaff, 2015: A consensus forecast for tropical cyclone gale wind radii. *Wea. Forecasting*, **30**, 1397–1403, doi:10.1175/WAF-D-15-0009.1.

——, J. L. Franklin, J. A. Knaff, and M. DeMaria, 2008: Experiments with a simple tropical cyclone intensity consensus. *Wea. Forecasting*, **23**, 304–312, doi:10.1175/2007WAF2007028.1.

——, P. A. Wittmann, and H. L. Tolman, 2010: Consistent tropical cyclone wind and wave forecasts for the U.S. Navy. *Wea. Forecasting*, **25**, 1293–1306, doi:10.1175/2010WAF2222376.1.

——, and Coauthors, 2012: Objective guidance for use in setting tropical cyclone conditions of readiness. *Wea. Forecasting*, **27**, 1052–1060, doi:10.1175/WAF-D-12-00008.1.

——, P. A. Wittmann, E. A. Serra, H. L. Tolman, J. Schauer, and T. Marchok, 2013: Evaluation of wave forecasts consistent with tropical cyclone warning center wind forecasts. *Wea. Forecasting*, **28**, 287–294, doi:10.1175/WAF-D-12-00060.1.

——, J. A. Hansen, P. A. Wittmann, J. A. Knaff, and A. Schumacher, 2016: Wave probabilities consistent with official tropical cyclone forecasts. *Wea. Forecasting*, **31**, 2035–2045, doi:10.1175/WAF-D-15-0093.1.

——, E. M. Fukada, J. A. Knaff, B. R. Strahl, M. J. Brennan, and T. Marchok, 2017: Tropical cyclone gale wind radii estimates for the western North Pacific. *Wea. Forecasting*, doi:10.1175/WAF-D-16-0196.1, in press.

Stewart, S. R., 2014: Hurricane Amanda (EP012014) 22–29 May 2014. National Hurricane Center Tropical Cyclone Rep., 15 pp. [Available online at http://www.nhc.noaa.gov/data/tcr/EP012014_Amanda.pdf.]

Tallapragada, V., and Coauthors, 2014: Hurricane Weather Research and Forecasting (HWRF) model: 2014 scientific documentation. Developmental Testbed Center, 105 pp. [Available online at http://www.dtcenter.org/HurrWRF/users/docs/scientific_documents/HWRFv3.6a_ScientificDoc.pdf.]

Trahan, S., and L. Sparling, 2012: An analysis of NCEP Tropical Cyclone Vitals and potential effects on forecasting models. *Wea. Forecasting*, **27**, 744–756, doi:10.1175/WAF-D-11-00063.1.

Uhlhorn, E. W., B. W. Klotz, T. Vukicevic, P. D. Reasor, and R. F. Rogers, 2014: Observed hurricane wind speed asymmetries and relationships to motion and environmental shear. *Mon. Wea. Rev.*, **142**, 1290–1311, doi:10.1175/MWR-D-13-00249.1.

Whitney, L. D., and J. S. Hobgood, 1997: The relationship between sea surface temperatures and maximum intensities of tropical cyclones in the eastern North Pacific Ocean. *J. Climate*, **10**, 2921–2930, doi:10.1175/1520-0442(1997)010<2921:TRBSST>2.0.CO;2.

Wilks, D. S., 2006: *Statistical Methods in the Atmospheric Sciences.* 2nd ed. Academic Press, 627 pp.

Wu, L., W. Tian, Q. Liu, J. Cao, and J. A. Knaff, 2015: Implications of the observed relationship between tropical cyclone size and intensity over the western North Pacific. *J. Climate*, **28**, 9501–9506, doi:10.1175/JCLI-D-15-0628.1.

Xu, J., and Y. Wang, 2010: Sensitivity of tropical cyclone inner-core size and intensity to the radial distribution of surface entropy flux. *J. Atmos. Sci.*, **67**, 1831–1852, doi:10.1175/2010JAS3387.1.